arXiv:1401.5610v1 [cond-mat.quant-gas] 22 Jan 2014

Stability of the Superfluid State in Three-Component Fermionic Optical Lattice Systems

Yuki Okanami, Nayuta Takemori, and Akihisa Koga
Department of Physics, Tokyo Institute of Technology, Meguro-ku, Tokyo 152-8551, Japan
(Dated: January 23, 2014)

Three-component fermionic optical lattice systems are investigated in dynamical mean-field theory for the Hubbard model. Solving the effective impurity model by means of continuous-time quantum Monte Carlo simulations in the Nambu formalism, we find that the s-wave superfluid state proposed recently is indeed stabilized in the repulsively interacting case and appears along the first-order phase boundary between the metallic and paired Mott states in the paramagnetic system. The BCS-BEC crossover in the three-component fermionic system is also addressed.

I. INTRODUCTION

Ultracold atomic systems provide a variety of interesting topics [1]. One of the most active topics is the superfluid (SF) state in ultracold fermions, which has widely been investigated since the observation of the crossover between the Bardeen-Cooper-Schrieffer (BCS) and the Bose-Einstein condensation (BEC) states [2–5]. The high controllability of interaction strength, particle number, and other parameters enables us to study pseudogap behavior [6, 7] and the SF state in other two-component fermionic systems such as the population-imbalanced and mass-imbalanced systems [8–10]. Recently, degenerate multi-component fermionic systems have experimentally been realized [11–15], which stimulates further theoretical investigation on the SF state in multi-component fermionic systems.

One of the simplest systems is the three-component fermionic optical lattice. Ground-state properties of the system have been studied in the Hubbard model where Mott transitions have been discussed in the paramagnetic case [16–18]. Recently, it has been suggested that the s-wave SF ground state is realized when two of three on-site repulsive interactions are strong [19]. This is contrast to the fact that the SF state in the two-component Hubbard model is stabilized by attractive interactions. Therefore, it is instructive to clarify whether or not the SF state realized in the three-component systems with repulsive interaction is adiabatically connected to that induced by the attractive interaction. In addition, it may be important to examine normal-state properties in the three-component system since the SF state is suggested to appear between the metallic and Mott states [19]. Hence, it is desired to study systematically particle correlations in the three-component interacting fermion systems.

For this purpose, we consider the three-component Hubbard model, combining dynamical mean-field theory (DMFT) [20–23] with a continuous-time quantum Monte Carlo (CTQMC) method [24, 25]. By calculating the pair potential, double occupancy, and renormalization factor, we determine finite-temperature phase diagrams of the system. The BCS-BEC crossover in the SF state is also discussed.

The paper is organized as follows. In Sec. II, we introduce the three-component Hubbard model and briefly summarize our theoretical approach. In Sec. III, we study grand-state properties in the paramagnetic case to discuss the competition between the metallic and Mott states. We then clarify the stability of the SF state at low temperatures in Sec. IV. A brief summary is given in the last section.

II. MODEL AND METHOD

We consider three-component fermions in an optical lattice, which should be described by the following Hubbard Hamiltonian,

$$\hat{\mathcal{H}} = -t \sum_{\langle i,j\rangle,\alpha} c^{\dagger}_{i\alpha} c_{j\alpha} + \frac{1}{2} \sum_{\alpha\neq\beta,i} U_{\alpha\beta} n_{i\alpha} n_{i\beta}, \qquad (1)$$

where $\langle i,j\rangle$ denotes the summation over the nearest neighbor sites, $c_{i\alpha}$ ($c^{\dagger}_{i\alpha}$) is the annihilation (creation) operator of a fermion with color $\alpha(=1,2,3)$ on the ith site, and $n_{i\alpha} = c^{\dagger}_{i\alpha} c_{i\alpha}$. Here, t is the transfer integral, and $U_{\alpha\beta}(=U_{\beta\alpha})$ is the on-site interaction between two fermions with colors α and β. For simplicity, we set $U_{12} \equiv U$ and $U_{23} = U_{31} \equiv U'$ and neglect the translational symmetry breaking phases such as the density wave and magnetically ordered states [19]. In the paper, we focus on the half-filled system with equally populations, setting the chemical potential as $\mu_\alpha = \sum_{\beta\neq\alpha} U_{\alpha\beta}/2$. We then consider the normal-state properties and the stability of the s-wave SF state. In the latter case, we assume that Cooper pairs are formed by the fermions with colors 1 and 2, and the pair potential $\Delta = \langle c_{i1} c_{i2}\rangle$ is regarded as an order parameter of the SF state.

First, we consider the symmetry of the Hamiltonian $\mathcal{H}(t, U_{12}, U_{23}, U_{31})$ at half filling. When the lattice is bipartite, we can use the particle-hole transformations [26] as $c_{j1} \to (-1)^j c^{\dagger}_{j1}, c_{j2} \to (-1)^j c^{\dagger}_{j2}$, and $c_{j3} \to c_{j3}$ and obtain the Hamiltonian $\mathcal{H}(t, U_{12}, -U_{23}, -U_{31})$. Therefore, our discussions can be restricted to the positive $U'(=U_{23}=U_{31})$ case without loss of generality. We

also note that the pair potential defined above is invariant under the transformation.

An important point is that the Hubbard model eq. (1) is reduced to interesting models in some limits, where ground state properties have been discussed. When $U = U'$, the system is reduced to the SU(3) Hubbard model, where the stability of the metallic and SF states has been discussed[16–18, 27–29]. In the case $U' = 0$, the system is divided into two systems: the two-component interacting fermions (colors 1 and 2) and free fermions (color 3). In the interacting fermions, a Mott transition occurs around $U/D \sim 3$ [30] while a pairing transition occurs around $U/D \sim -3$ [31] in the paramagnetic state. If one allows the ordered state with translational symmetry, the SF ground state is always stabilized in the attractive case [32–34]. When the interaction is anisotropic ($U \neq U'$), the existence of the s-wave SF state in repulsively interacting case has been clarified [19]. This SF state is realized in a certain region between the metallic and Mott states, and thereby it is necessary to treat the competing phases carefully. However, the treatment might be simple to discuss the quantum phase transitions correctly, *e.g.* the iterative perturbation theory based on the second-order perturbation sometimes underestimates particle correlations [30], and the single-site self-energy functional theory should be difficult to study the first-order transitions quantitatively [35]. Furthermore, it is still unclear how this SF state is adiabatically connected to the conventional SF state described by the BCS theory. Therefore, it is desired to discuss systematically the stability of the SF state in the three-component fermionic Hubbard model.

Before discussions, we consider the stability of the SF state by means of the simple mean-field theory. When the static mean-field Δ is introduced, the effective Hamiltonian is given by $\hat{\mathcal{H}}_{BCS} = -t\sum_{\langle i,j\rangle,\alpha} c^{\dagger}_{i\alpha}c_{j\alpha} + U\sum_i \left(\Delta^* c_{i1}c_{i2} + h.c.\right)$. We note that the interaction U' is irrelevant and fermions with color 3 play no role in stabilizing the SF state. In the case, the s-wave SF state is stabilized only when the interaction is attractive ($U < 0$). On the other hand, in the repulsive case ($U > 0$), fermions with color 1 and 2 have no chance to form Cooper pairs, which is contrast to the previous work [19]. Furthermore, this theory is not appropriate to access the strong coupling region, where the Mott state should be stabilized. Therefore, it is necessary to incorporate particle correlations correctly.

To this end, we make use of DMFT [20–23]. In DMFT, the original lattice model is mapped to an effective impurity model, where local and dynamical correlations can be taken into account. The lattice Green's function is obtained via a self-consistency condition imposed on the impurity problem. This allows us to discuss the stability of the s-wave SF state more quantitatively beyond the static BCS mean-field theory [36]. In fact, the DMFT method has successfully been applied to various strongly correlated fermion systems with the SF or superconducting states [32, 37–43].

When the SF state is treated in the framework of DMFT, the impurity Green's function for the effective model $\hat{G}_{\rm imp}(\tau)$ should be described by a 3×3 matrix as,

$$\hat{G}_{\rm imp}(\tau) = \begin{pmatrix} G_1(\tau) & F(\tau) & 0 \\ F^*(\tau) & -G_2(-\tau) & 0 \\ 0 & 0 & G_3(\tau) \end{pmatrix}, \qquad (2)$$

where $G_\alpha(\tau) = -\langle T_\tau f_\alpha(\tau) f^{\dagger}_\alpha(0)\rangle$ denotes the normal Green's function for color α, and $F(\tau) = -\langle T_\tau f_1(\tau) f_2(0)\rangle$ and $F^*(\tau) = -\langle T_\tau f^{\dagger}_2(\tau) f^{\dagger}_1(0)\rangle$ denote the anomalous Green's functions. In the calculations, we use a semi-circular density of states, $\rho(x) = 2/(\pi D)\sqrt{1-(x/D)^2}$, where D is the half bandwidth. The self-consistency equation is given by

$$\hat{G}^{-1}_{0,\rm imp}(i\omega_n) = i\omega_n\hat{1} + \hat{\mu} - \left(\frac{D}{2}\right)^2 \hat{\Lambda}\hat{G}_{\rm imp}(i\omega_n)\hat{\Lambda}, \qquad (3)$$

where $\hat{1}$ is the identity matrix, $\hat{\mu} = {\rm diag}(\mu_1, -\mu_2, \mu_3)$, $\hat{\Lambda} = {\rm diag}(1,-1,1)$, $\omega_n = (2n+1)\pi T$ is the Matsubara frequency, and T is the temperature. Here, $\hat{G}_{0,\rm imp}$ and $\hat{G}_{\rm imp}$ are noninteracting and full Green's functions for the effective impurity model.

There are various methods to solve the effective impurity problem. To study the stability of the SF state in a three-component fermionic optical lattice system, an unbiased and accurate numerical solver is necessary such as an exact diagonalization [44] and the numerical renormalization group [46, 47]. A particularly powerful method for exploring finite-temperature properties is the hybridization-expansion CTQMC method [24, 25]. This enables us to study the Hubbard model in both weak- and strong-coupling regimes.

In this paper, we use the half bandwidth D as a unit of energy. We calculate the double occupancy for colors α and β $D_{\alpha\beta}$, pair potential Δ, internal energy E, and specific heat C, which are given by

$$D_{\alpha\beta} = \langle n_{i\alpha}n_{i\beta}\rangle, \qquad (4)$$

$$\Delta = \langle c_{i1}c_{i2}\rangle = \lim_{\tau\to 0_+} F(\tau), \qquad (5)$$

$$E = \left(\frac{D}{2}\right)^2 \int_0^\beta d\tau {\rm Tr}[\hat{\rm G}_{\rm imp}(\tau)\hat{\Lambda}\hat{\rm G}_{\rm imp}(-\tau)\hat{\Lambda}] + \frac{1}{2}\sum_{\alpha\beta} U_{\alpha\beta}D_{\alpha\beta}, \qquad (6)$$

$$C = \frac{dE}{dT}. \qquad (7)$$

We also calculate the quantity $Z_\alpha = [1 - {\rm Im}\Sigma_\alpha(i\omega_0)/\omega_0]^{-1}$ as the quasi-particle weight at finite temperatures, where Σ_α is the normal self-energy for color α. In addition to these static quantities, we compute the density of states, applying the maximum entropy method (MEM) [48–50] to the normal Green's function. We then discuss how the gap structure appears around the Fermi level at low temperatures.

III. LOW-TEMPERATURE PROPERTIES IN THE PARAMAGNETIC STATE

In the section, we consider low-temperature properties of the half-filled system in the paramagnetic state. Then we study quantitatively how the Mott and pairing transitions in the two-component Hubbard model are connected to the phase transitions in the three-component systems [17, 18]. By performing DMFT with CTQMC method, we calculate the double occupancies $D_{\alpha\beta}$ and renormalization factors Z_α at the temperature $T/D = 0.015$, as shown in Fig. 1. First, we consider

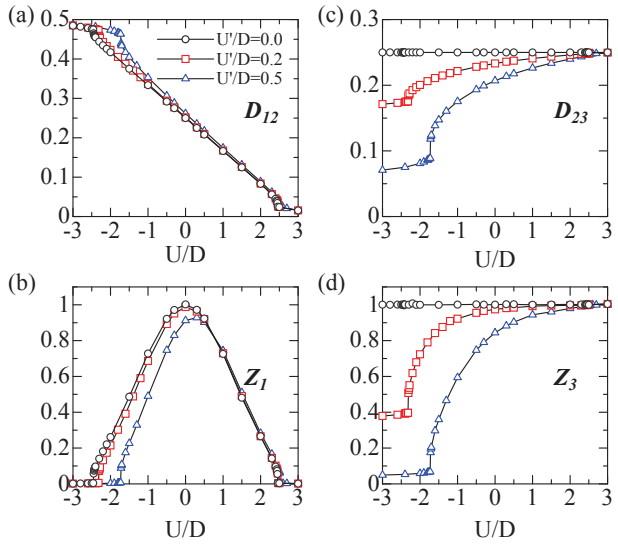

FIG. 1: (Color online). Double occupancies $D_{\alpha\beta}$ and the renomalization factors Z_α as functions of U/D at $T/D = 0.015$. Open circles, squares and triangles represent the results for the half-filled system with $U'/D = 0.0$, 0.2 and 0.5.

the system with $U' = 0$, which is divided into two systems: two-component interacting fermions (colors 1 and 2) and free fermions (color 3). Now, we focus on the two-component fermions. As decreasing interaction U from zero, we find that the double occupancy D_{12} is smoothly increased and the renormalization factor Z_1 is decreased as shown in Figs. 1 (a) and (b). In the weak-coupling region ($U_p < U$), the metallic state is realized with a finite renormalization factor, where $U_p/D \sim -2.6$. At $U = U_p$, the jump singularity appears in both curves and the first-order phase transition occurs. When $U < U_p$, each site is doubly occupied or empty ($D_{12} \sim 0.5$), and the state is specified by the pairing state [31]. On the other hand, the increase in the interaction $U(> 0)$ decreases both D_{12} and Z_1 and induces the phase transition at $U_m/D \sim 2.6$. When $U_m < U$, each site is singly occupied ($D_{12} \sim 0.0$), which implies that the Mott insulating state is realized. We also find that these quantities are symmetric at $U = 0.0$, which is reflected by the fact that the repulsive Hubbard model is equivalent to the attractive one under the particle-hole transformation [26]. In contrast to the two-component system, fermions with color 3 are always noninteracting, and thereby $D_{23} = 0.25$ and $Z_3 = 1.0$.

The introduction of the interaction U' leads to a drastic change in fermions with color 3, in particular, when $U < 0$. A clear jump singularity appears in the curves of the double occupancy D_{23} and the renormalization factor Z_3 at $U_p/D \sim -2.4$ while a tiny one appears around $U_m/D \sim 2.6$ in the case $U'/D = 0.2$. When $U_p < U < U_m$, metallic behavior still remains with finite renormalization factors Z_α ($\alpha = 1, 2, 3$). In the large $U(> U_m)$ region, we find that $D_{12} \sim 0$, $D_{23} = D_{31} \sim 0.25$, $Z_1 = Z_2 \sim 0.0$ and $Z_3 \sim 1.0$. This implies that the Mott insulating state is realized for colors 1 and 2, and free fermion behavior survives for color 3. Therefore, this state can be regarded as the color selective Mott (CSM) state [17]. By contrast, when $U < U_p$, D_{23} and Z_3 are rapidly decreased on the introduction of the interaction U', as shown in Figs. 1 (c) and (d). This suggests that metallic behavior for fermions with color 3 is no longer stable at zero temperature although the renormalization factor Z_3 is not so small at $T/D = 0.015$. To confirm this, we also calculate the temperature dependence of the renormalization factor Z_3, as shown in Fig. 2. It is found that in the system with $U/D = -3.0$ and

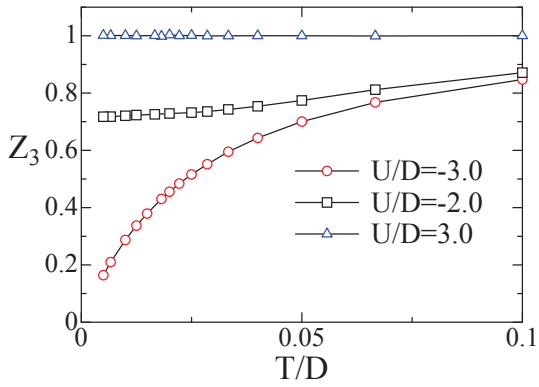

FIG. 2: (Color online) Open circles, squares and triangles represent the renormalization factor Z_3 in the system with a fixed $U'/D = 0.2$ when $U/D = -3.0$, -2.0 and 3.0.

$U'/D = 0.2$, the renormalization factor decreases with lowering temperatures and does not converge down to $T/D = 0.005$. This tendency suggests that the paired Mott (PM) ground state [17] is realized with $Z_\alpha \sim 0.0$, $D_{12} \sim 0.5$, and $D_{23} \sim 0.0$ and bad metallic behavior appears at intermediate temperatures. On the other hand, in the case $U/D = -2.0$ ($U/D = 3.0$), the renormalization factor Z_3 becomes constant at low temperatures, which is consistent with the fact that the metallic (CSM) ground state is realized.

By performing similar calculations, we obtain the phase diagram for the paramagnetic state at $T/D = 0.015$, as shown in Fig. 3. We find that four quantum states compete with each other, such as CSM, metallic,

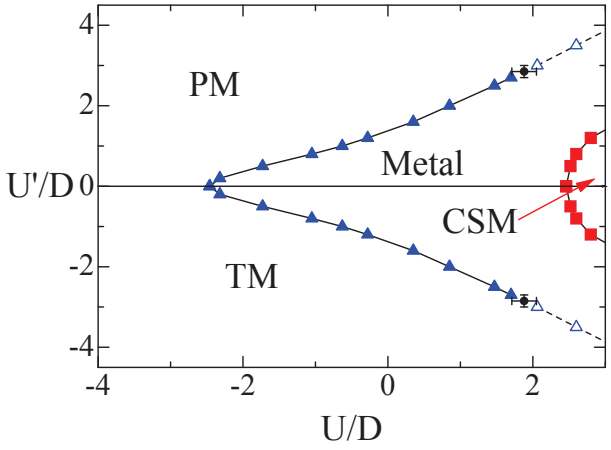

FIG. 3: (Color online) Phase diagram at $T/D = 0.015$ in the paramagnetic system. Squares (triangles) represent the first-order phase transition points between the metallic and CSM (PM or TM) states, and Circles indicate the critical end points. Dash lines represent the crossover between the PM (TM) and metallic states.

PM and trion Mott (TM) states. Last two states are equivalent under the particle-hole transformations and the TM state is realized only when U' is negative. In the region with $U/D \lesssim -2.6$ and small $|U'|$, fermions with colors 1 and 2 strongly couple with each other due to the attractive interaction, and fermions with color 3 weakly couple with the other fermions. Therefore, bad metallic behavior appears at the temperature, as discussed above. This state is adiabatically connected to the PM or TM state. Since the PM and TM states are stabilized by the interaction strength $|U'|$ at low temperatures, the first-order phase transition point U_p is rapidly increased, as shown in Fig. 3. In the large U' region, the singularity in the physical quantities at the phase boundary smears. We find the critical end point around $(U/D, U'/D) \sim (1.9, 2.9)$. Beyond the point, one finds no singularities and the crossover between the PM and metallic states occurs. By contrast, the other transition point U_m is insensitive to the interaction U'. This may originate from the nature of the CSM state. In the state, a fermion with color 1 or 2 is singly occupied at each site, and fermions with color 3 are almost free. Therefore, the introduction of the interaction U' little affects low-temperature properties in the system.

In the section, we have discussed the competition between the CSM, metallic, PM, and TM states in the paramagnetic system. In the following, we study how the s-wave SF state is realized between the metallic and PM states and how the BCS-BEC crossover occurs in the system.

IV. STABILITY OF THE SUPERFLUID STATE

In this section, we perform DMFT in the Nambu formalism to discuss how the SF state is realized in the system at low temperatures. When $U' = 0.0$, the system is reduced to the two-component Hubbard model, where the SF state is realized in the case $(-18 < U/D < -0.55)$ at $T/D = 0.015$. It is known that the BCS-BEC crossover, which is roughly characterized by the maximum of the pair potential, occurs around $U/D \sim -5.0$ [40]. When the system is in the strong-coupling BEC region $(U/D = -7.0,\ U' = 0.0)$, the introduction of the interaction U' monotonically decreases the pair potential, and finally it suddenly vanishes at $U'/D = 0.4$, as shown in Fig. 4. Jumps are also found in the curves of the double occupancy and renormalization factor although the singularities may be invisible in Fig. 5. Therefore, we can say that in the BEC region, the first-order phase transition occurs to the PM state. Similar behavior is also found in the BCS-BEC crossover region $(U/D = -5.0,\ U' = 0.0)$, where the first-order phase transition occurs at $U'/D = 0.47$. On the other hand, in the weak-coupling BCS region $(U/D = -1.0,\ U' = 0.0)$, different behavior appears in the pair potential, as shown in Fig. 4, although we can not find an obvious change in the other quantities as shown in Fig. 5. Namely, the pair potential has a maximum around $U'/D \sim 0.6$, as shown in Fig. 4. This implies that the introduction of the interaction U' stabilizes the SF state and induces the BCS-BEC crossover. Then, the first-order phase transition occurs from the BEC-type SF state to the PM state at $U'/D = 0.97$. This nonmonotonic behavior is more clearly found in the positive U case. When $U' = 0$, the SF state is no longer realized. As increasing U', the metallic state becomes unstable and the second-order phase transition occurs to the BCS-type SF state with the pair potential. By examining critical behavior $\Delta \sim |U - U_c|^{\beta}$

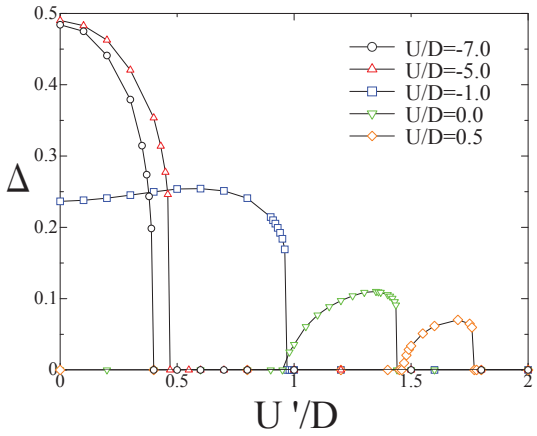

FIG. 4: (Color online) Pair potential Δ as functions of U'/D in the system at $T/D = 0.015$ when $U/D = -7.0, -5.0, -1.0$, 0.0, and 0.5.

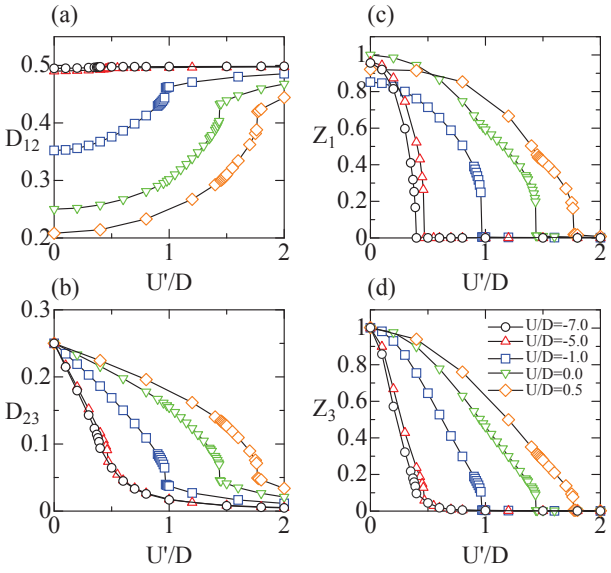

FIG. 5: (Color online) Double occupancies $D_{\alpha\beta}$ and renormalization factors Z_α at $T/D = 0.015$ when $U/D = -7.0$, -5.0, -1.0, 0.0, and 0.5.

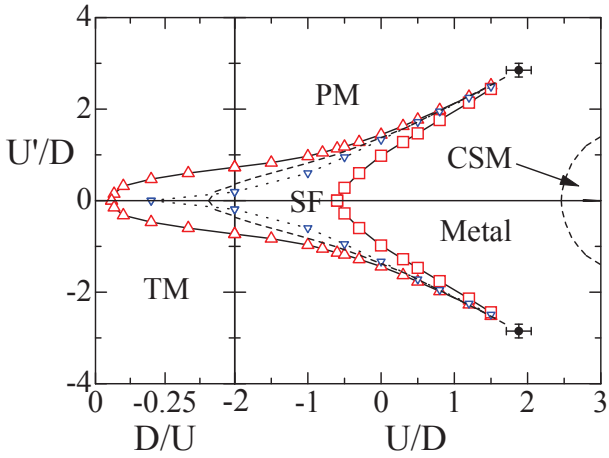

FIG. 6: (Color online) Phase diagram of the system at $T/D = 0.015$. Triangles (squares) represent the phase transition points between the SF and PM (metallic) states. The dashed lines represent the phase boundaries in the paramagnetic system. Dotted lines indicate the ridges of the pair potential in the SF state. (please delete inverted triangles)

with the exponent $\beta = 1/2$, we determine the critical interactions $U'/D \sim 0.98$ ($U = 0.0$) and $U'/D \sim 1.47$ ($U/D = 0.5$) at $T/D = 0.015$. Further increase of U' stabilizes the SF state, and finally the first-order phase transition occurs to the PM state at $U'/D = 1.44$ ($U = 0.0$) and $U'/D = 1.77$ ($U/D = 0.5$). An important point is that the SF state is realized even when all on-site interactions are repulsive. These indicate that the interaction U' plays an essential role in stabilizing the SF state in the repulsively interacting case since the s-wave SF state does not appear in the two-component repulsive Hubbard model.

By performing similar calculations for different values of U and U', we obtain the phase diagram at the temperature $T/D = 0.015$ as shown in Fig. 6. When $U' = 0.0$, the system is reduced to the two-component Hubbard model for colors 1 and 2. In the BEC (strong-coupling) region, the introduction of the interaction U' drives the system to the PM state, and its phase transition is of first order. On the other hand, in the BCS (weak-coupling) region, the phase transition between the SF and metallic states is of second order. A remarkable point is that the SF state emerges along the phase boundary between the metallic and PM states discussed in the previous section and persists up to fairly large repulsive interactions. Therefore, we can say that the SF state in the repulsive case is adiabatically connected to the trivial SF state realized in the two-component attractive Hubbard model. On the other hand, once the parameters (U, U') are away from the line, the SF state becomes immediately unstable. These mean that the SF state in the repulsively interacting case is induced by the competition between the on-site interactions U and U'. In the stronger coupling region, the SF state is no longer stable, and the phase diagram is reduced to the paramagnetic one, where the PM, metallic, and CSM states compete with each other (see Fig. 3). We wish to note that the critical end point for the SF state corresponds to that in the paramagnetic phase diagram within our numerical accuracy. Therefore, we can say that the first-order phase transition between the PM and metallic states in the paramagnetic system plays an essential role in stabilizing the SF state. This is different from the origin of the weak-coupling SF state discussed in terms of the random phase approximation [19]. Although we have determined the phase diagram at the temperature $T/D = 0.015$, these results suggest that the SF state is stabilized in the stronger coupling region ($U' \gtrsim U \gg D$) at lower temperatures.

We also consider the BCS-BEC crossover in the three-component system. This crossover should occur around the ridges of the pair potential in the parameter space (U, U'), except for the $U' = 0.0$ axis. Here, we examine low-temperature properties characteristic of the BCS and BEC regions. The system with $U/D = -1.0$ and $U'/D = 0.9$ belongs to the BEC-type SF state close to the first-order phase boundary at $T/D = 0.015$. The temperature dependence of physical quantities are shown in Fig. 7. We find a jump singularity in each curve at the temperature $T_c/D = 0.024$, which means the existence of the first-order phase transition. Above the temperature, double occupancies and renormalization factors are calculated as $D_{12} \sim 0.5$, $D_{23} \sim 0.0$, and $Z_\alpha \sim 0.0$, and the PM state is indeed stabilized. The entropy for the PM state should be larger than that for the SF state at $T = T_c$, yielding the discontinuity in the curve of the internal energy. Therefore, we can find that the peak in the specific heat below the critical temperature is somewhat

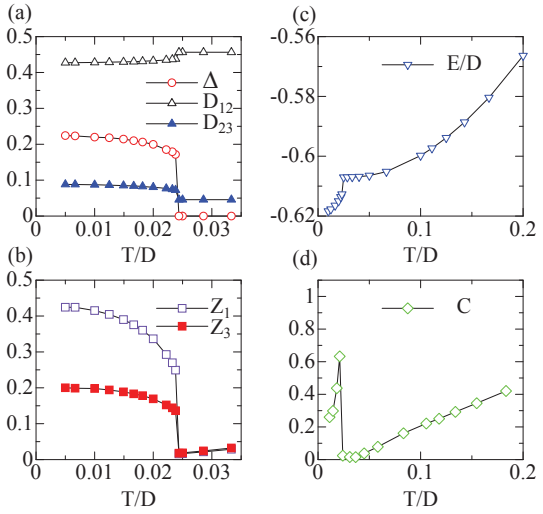

FIG. 7: (Color online) The temperature dependence of the pair potential, double occupancies, renormalization factors, internal energy, and specific heat when $U/D = -1.0$ and $U'/D = 0.9$.

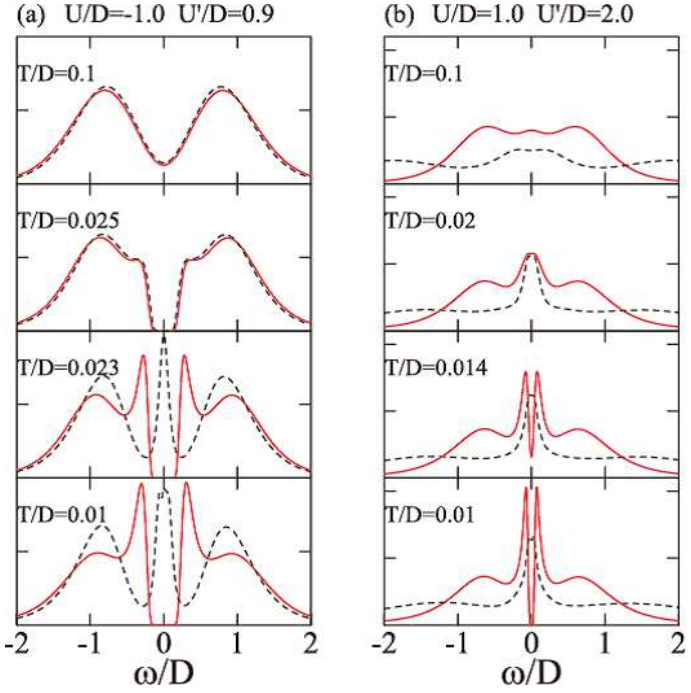

FIG. 8: (Color online) Solid (dashed) lines represent the density of states for fermions with colors 1 (color 3) when $U/D = -1.0$ and $U'/D = 0.9$ (a), and $U/D = 1.0$ and $U'/D = 2.0$ (b).

smaller than that expected in the conventional s-wave SF state. We also deduce the density of states by means of the MEM [48–50], as shown in Fig. 8 (a). In the BEC region, paired particles are formed even above the transition temperature, stabilizing the PM state. Therefore, the large gap structure, which is proportional to the strength of the on-site interactions, appears in the density of states for each color. The sudden increase in the pair potential leads to interesting behavior in dynamical properties. The large gap and sharp peaks at its edges appear in the density of states for colors 1 and 2. On the other hand, the sharp peak structure is induced at the Fermi level in the density of states for color 3, as shown in Fig. 8 (a). Therefore, below the transition temperature, paired particles are condensed, and the heavy metallic behavior appears for fermions with color 3. Since the phase transition is accompanied with the insulator-metal transition for fermions with color 3, low-temperature properties are different from those in the BEC region of the two-component system, where the second-order phase transition occurs [40]. Therefore, we can say that the BEC region in the three-component system should be characteristic of the first-order phase transition.

In the BCS case ($U/D = 1.0$ and $U'/D = 2.0$), different behavior appears, as shown in Fig. 9. We find that the decrease of the temperature induces the second-order phase transition. The critical temperature is deduced as $T/D \sim 0.017$, by examining critical behavior of the pair potential $\Delta \sim |T - T_c|^{\beta}$. There is no discontinuity in the curve of the internal energy and the large specific heat appears below the critical temperature, in contrast to the BEC-type case. We clearly find the local minimum in the specific heat around $T^*/D \sim 0.05$.

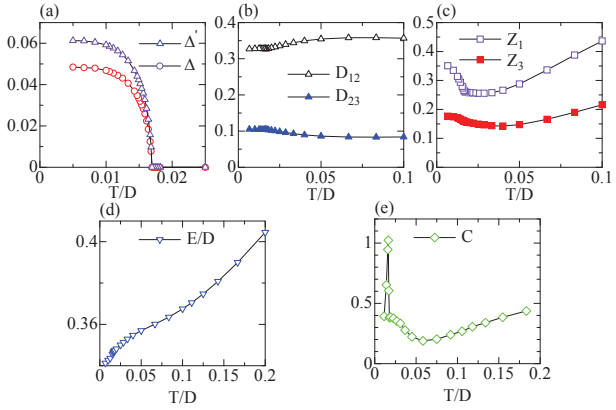

FIG. 9: (Color online) Temperature dependence of the pair potential, double occupancies, renormalization factors, internal energy, and specific heat when $U/D = 1.0$ and $U'/D = 2.0$.

This behavior may be explained by the following. At the higher temperature $T > T^*$, the strength of the interaction affects low-energy properties and gap behavior appears, where the renormalization factors are decreased on the decrease of the temperature. Around $T = T^*$, the competition between on-site interactions begins to form the quasiparticles around the Fermi level, giving rise to the minimum of the renormalization factors and specific heat, as shown in Figs. 9 (c) and (e). This is more clearly

found in the density of states, as shown in Fig. 8 (b). At high temperatures, gap behavior appears in the density of states for each color and the quasiparticle peaks develop on the decreasing temperatures. Once the system enters the SF state, in the spectral functions with colors 1 and 2, a dip structure develops at the Fermi level while a sharp quasiparticle peak remains in the other. These low-temperature properties are contrast to those in the BEC region.

When the parameters (U, U') are varied in the SF state, the crossover occurs between the BCS-type and BEC-type SF states, and low-temperature properties are gradually changed. We find that the phase transition from the BEC-type (BCS-type) SF state to the paramagnetic state is of first (second) order.

Before closing this section, we briefly discuss the effect of the repulsive interaction on the SF state. When $U/D = 1.0$ and $U'/D = 2.0$, the anomalous Green's function $F(\tau)$ at the low temperature $T/D = 0.01$ is shown in Fig. 10. We find that the anomalous Green's function takes its maximum value Δ' away from $\tau = 0$. This is contrast to the conventional anomalous Green's function in the SF state, where the maximum is located at $\tau = 0$ and its value can be regarded as the order parameter, as shown in Fig. 10. This may originate from the fact that the repulsive interaction between fermions with colors 1 and 2 tends to break the Cooper pair at each site. To clarify how such a nontrivial structure in $F(\tau)$ appears below the critical temperature, we also show the temperature dependence of the maximum value Δ' in Fig. 9 (a). As decreasing temperature, Δ and Δ' are simultaneously induced at the critical temperature and are gradually increased at lower temperatures. Since the ratio $\Delta'/\Delta \sim 1.3$ little depends on the temperature, the SF state without the pair potential $[F(\tau) \neq 0, \Delta = 0]$ should not be realized at any temperatures in the three-component system.

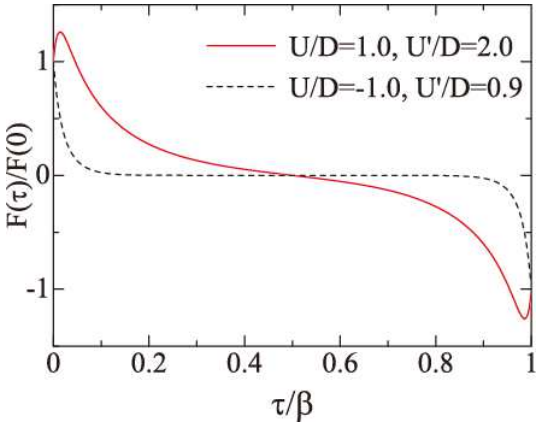

FIG. 10: (Color online) Solid (dashed) line represents the normalized anomalous green's function at $T/D = 0.01$ when $U/D = 1.0, U'/D = 2.0$ $(U/D = -1.0, U'/D = 0.9)$.

V. CONCLUSIONS

We have investigated the three-component Hubbard model in infinite dimensions, combining DMFT with the CTQMC method. Computing the double occupancy and renormalization factor, we have determined the finite-temperature phase diagram in the paramagnetic state. It has been clarified that the PM, CSM, TM, and metallic states compete with each other in the system. We have also studied the stability of the SF state and have confirmed that the SF state is indeed stabilized in the repulsively interacting case. Systematic calculations have revealed that this state is adiabatically connected to the SF state realized in the two-component attractive Hubbard model. Moreover, we have studied low-temperature properties in the BCS and BEC regions. It is found that the BCS state is characterized by the second-order phase transition, while the BEC state is by the first-order one. This is contrast to the two-component system, where the second-order phase transitions occur in both limits. It is also interesting how the SF state is realized in the multi-component fermionic systems for lithium and ytterbium atoms, which is now under consideration.

Acknowledgments

The authors thank K. Inaba and S. Suga for valuable discussions. This work was partly supported by the Grant-in-Aid for Scientific Research 20740194 (A.K.) and the Global COE Program "Nanoscience and Quantum Physics" from the Ministry of Education, Culture, Sports, Science and Technology (MEXT) of Japan. N.T. also acknowledges the financial support from the Global Center of Excellence Program by MEXT, Japan through the "Nanoscience and Quantum Physics" Project of the Tokyo institute of Technology. The simulations have been performed using some of the ALPS libraries [51].

[1] I. Bloch, J. Dalibard and S. Nascimbène, Nat. Phys. **8**, 267 (2012).
[2] C. A. Regal, M. Greiner, and D. S. Jin, Phys. Rev. Lett. **92**, 040403 (2004).
[3] M. Bartenstein, A. Altmeyer, S. Riedl, S. Jochim, C. Chin, J. Hecker Denschlag, and R. Grimm, Phys. Rev. Lett. **92**, 120401 (2004).
[4] M. W. Zwierlein, C. A. Stan, C. H. Schunck, S. M. F. Raupach, A. J. Kerman, and W. Ketterle, Phys. Rev. Lett. **92**, 120403 (2004).
[5] J. Kinast, S. L. Hemmer, M. E. Gehm, A. Turlapov, and J. E. Thomas, Phys. Rev. Lett. **92**, 150402 (2004).

[6] J. T. Stewart, J. P. Gaebler, and D. S. Jin, Nature (London) **454**, 744 (2008).

[7] J. P. Gaebler, J. T. Stewart, T. E. Drake, D. S. Jin, A. Perali, P. Pieri, and G. C. Strinati, Nat. Phys. **6**, 569 (2010).

[8] M. W. Zwierlein, A. Schirotzek, C. H. Schunck, and W. Ketterle, Science **311**, 492 (2006).

[9] M. Taglieber, A. -C. Voigt, T. Aoki, T. W. Hänsch, and K. Dieckmann, Phys. Rev. Lett. **100** 010401 (2008).

[10] H. Hara, Y. Takasu, Y. Yamaoka, J. M. Doyle, and Y. Takahashi, Phys. Rev. Lett. **106** 205304 (2011).

[11] T. B. Ottenstein, T. Lompe, M. Kohnen, A. N. Wenz, and S. Jochim, Phys. Rev. Lett. **101** 203202 (2008).

[12] J. H. Huckans, J. R. Williams, E. L. Hazlett, R. W. Stites, and K. M. O'Hara, Phys. Rev. Lett. **102** 165302 (2009).

[13] T. Fukuhara, Y. Takasu, M. Kumakura, and Y. Takahashi, Phys. Rev. Lett. **98**, 030401 (2007).

[14] S. Taie, Y. Takasu, S. Sugawa, R. Yamazaki, T. Tsujimoto, R. Murakami, and Y. Takahashi, Phys. Rev. Lett. **105**, 190401 (2010).

[15] B. J. DeSalvo, M. Yan, P. G. Mickelson, Y. N. Martinez de Escobar, and T. C. Killian, Phys. Rev. Lett. **105**, 030402 (2010).

[16] E. V. Gorelik and N. Blümer, Phys. Rev. A **80**, 051602(R) (2009).

[17] K. Inaba, S. Miyatake, and S. Suga, Phys. Rev. A **82**, 051602(R) (2010).

[18] S. Miyatake, K. Inaba, and S. Suga, Phys. Rev. A **81**, 021603(R) (2010).

[19] K. Inaba and S. Suga, Phys. Rev. Lett. **108**, 255301 (2012); K. Inaba and S. Suga, Mod. Phys. Lett B **27** 1330008 (2013).

[20] W. Metzner and D. Vollhardt, Phys. Rev. Lett. **62**, 324 (1989).

[21] E. Müller-Hartmann, Z. Phys. B **74**, 507 (1989).

[22] A. Georges, G. Kotliar, W. Krauth, and M. J. Rozenberg, Rev. Mod. Phys. **68**, 13 (1996).

[23] T. Pruschke, M. Jarrell, and J. K. Freericks, Adv. Phys. **44**, 187 (1995).

[24] E. Gull, A. J. Millis, A. N. Rubtsov, A. I. Lichtenstein, M. Troyer, and P. Werner, Rev. Mod. Phys. **83**, 349 (2011).

[25] P. Werner, A. Comanac, L. de Medici, M. Troyer, and A. J. Millis, Phys. Rev. Lett. **97**, 076405 (2006).

[26] H. Shiba, Prog. Theor. Phys. **48**, 2171 (1972).

[27] C. Honerkamp and W. Hofstetter, Phys. Rev. Lett. **92**, 170403 (2004); C. Honerkamp and W. Hofstetter, Phys. Rev. B **70**, 094521 (2004).

[28] A. Rapp, G. Zaránd, C. Honerkamp, and W. Hofstetter, Phys. Rev. Lett. **98**, 160405 (2007); A. Rapp, W. Hofstetter, and G. Zaránd, Phys. Rev. B **77**, 144520 (2008).

[29] K. Inaba and S. Suga, Phys. Rev. A **80**, 041602(R) (2009).

[30] A. Georges and W. Krauth, Phys. Rev. B **48**, 7167 (1993).

[31] M. Capone, C. Castellani, and M. Grilli, Phys. Rev. Lett. **88**, 126403 (2002).

[32] A. Garg, H. R. Krishnamurthy, and M. Randeria, Phys. Rev. B **72**, 024517 (2005).

[33] J. Bauer, A. C. Hewson, and N. Dupuis, Phys. Rev. B **79**, 214518 (2009); J. Bauer and A. C. Hewson, Europhys. Lett. **85**, 27001 (2009).

[34] A. Toschi, M. Capone, and C. Castellani, Phys. Rev. B **72**, 235118 (2005); A. Toschi, P. Barone, M. Capone, and C. Castellani, New J. Phys. **7**, 7 (2005).

[35] M. Potthoff, Eur. Phys. J. B **36**, 335 (2003).

[36] A. Georges, G. Kotliar, and W. Krauth, Z. Phys. B **92**, 313 (1993).

[37] T.-L. Dao, M. Ferrero, A. Georges, M. Capone, and O. Parcollet, Phys. Rev. Lett. **101**, 236405 (2008).

[38] A. Koga and P. Werner, J. Phys. Soc. Jpn. **79**, 064401 (2010); J. Phys. Soc. Jpn. **79** 114401 (2010).

[39] S. Hoshino and Y. Kuramoto, arXiv:1309.5719.

[40] A. Koga and P. Werner, Phys. Rev. A **84**, 023638 (2011).

[41] K. Haule and G. Kotliar, Phys. Rev. B **76**, 104509 (2007).

[42] N. Takemori and A. Koga, J. Phys. Soc. Jpn. **81**, 063002 (2012).

[43] O. Bodensiek, R. Zitko, M. Vojta, M. Jarrell, and T. Pruschke, Phys. Rev. Lett. **110**, 146406 (2013).

[44] M. Caffarel and W. Krauth, Phys. Rev. Lett. **72**, 1545 (1994).

[45] A. Privitera, M. Capone, and C. Castellani, Phys. Rev. B **81**, 014523 (2010).

[46] H. R. Krishna-murthy, J. W. Wilkins, and K. G. Wilson, Phys. Rev. B **21**, 1003 (1980).

[47] R. Bulla, T. Costi, and Th. Pruschke, Rev. Mod. Phys. **80**, 395 (2008).

[48] S. F. Gull, in *Maximum Entropy and Bayesian Methods in Science and Engineering*, ed. G. J. Erickson and C. R. Smith (Kluwer Academic, Dordrecht, 1988) p. 53; J. Skilling(Kluwer Academic, Dordrecht, 1989) p. 45; S. F. Gull, *ibid*. p. 53.

[49] R. N. Silver, D. S. Sivia and J. E. Gubernatis, Phys. Rev. B **41**, 2380 (1990); J. E. Gubernatis, M. Jarrell, R. N. Silver and D. S. Sivia, Phys. Rev. B **44**, 6011 (1991).

[50] W. F. Press, S. A. Teukolsky, W. T. Vetterling and B. R. Flannery, *Numerical Recipes* (Cambridge University Press, Cambridge, 1992) p. 809.

[51] A. F. Albuquerque, F. Alet, P. Corboz, P. Dayal, A. Feiguin, S. Fuchs, L. Gamper, E. Gull, S. Gurtler, A. Honecker, R. Igarashi, M. Korner, A. Kozhevnikov, A. Lauchli, S. R. Manmana, M. Matsumoto, I. P. McCulloch, F. Michel, R. M. Noack, G. Paw.owski, L. Pollet, T. Pruschke, U. Schollwock, S. Todo, S. Trebst, M. Troyer, P. Werner, S. Wessel, J. Magn. Magn. Mater. **310**, 1187 (2007).